High-speed and high-accuracy algorithm for cloud detection and its application

SHAN Na[1,2], ZHENG Tian-yao[1], WANG Zhen-song[1]

1. *Institute of Computing Technology, Chinese Academy of Sciences, Beijing* 100190, *China*;
2. *Graduate University of Chinese Academy of Sciences, Beijing* 100190, *China*

Abstract: The cloud cover is an important factor which lowers the remote sensing image quality, so real-time automatic cloud detection and effective rejection of high cloud coverage pictures are of prime importance. In this paper we proposed a high performance and high accuracy algorithm of cloud detection which combines two different analytical techniques: the spectrum threshold comparison and the texture analysis. These two approaches discriminate the image from different visions. A structure of the discrimination tree is proposed to improve the accuracy and to accelerate the detecting procedure, which defines the rule how to use these two methods properly. The cloud detection results gained by this algorithm are well satisfied. And the structure of the discrimination tree promotes the operating efficiency on average. We also proposed an advanced approach to calculate the fractal dimension value, which is about five times faster than the original approach. The cloud detection algorithm has been applied to the data processing system of China-Brazil Earth Resources Satellite-2B. The experimental results show that this algorithm can satisfy the demand of error rate: the false alarm rate is lower than 5% and the missed detection rate is lower than 10%.

Key words: satellite remote sensing image, cloud detection, fractal dimension calculation, gray level co-occurrence matrix, structure of the discrimination tree

CLC number: TP751.1 **Document code:** A

1 INTRODUCTION

The remote sensing images acquired by space-borne optical remote sensing systems have been applied to many fields such as meteorological observation and forecast, Earth resources surveys, environmental contamination detection, natural disasters monitoring and so on. During the process of the remote sensing imaging it is hard to obtain complete clear images without cloud. The presence of cloud may obstruct the use of certain image data, for the information of objects on the earth is lost because of the cloud coverage. This will influence the analysis and interpretation of the images as well. Therefore, a real-time cloud detection process is required to distinguish the parts covered by cloud from the parts cloudless. And rejecting the cloudy parts of the images can obtain better utilization of expensive satellite resources such as storage device and downlink bandwidth. In nature, there are a great variety of clouds, and their texture features are random. These diversities are mainly caused by the geographical positions, seasons, climate, etc. So cloud detection is a difficult problem in the field of remote sensing image processing. A lot of cloud detection algorithms have been proposed. The theory of early approaches is based on the observation that clouds are highly reflection and cold. These approaches compare the gray levels of pixels with a threshold value to distinguish clouds and objects. At present, many researchers study higher accuracy cloud detection algorithms based on the threshold comparison method, such as homomorphic filtering (Li *et al*., 2003), statistical analysis, clustering (Liu *et al*., 2007;Wang *et al.*, 2006), multi-spectral analysis (Loyola, 1998; Song & Zhao, 2003), etc. Other researchers propose the texture analysis (Yu *et al*., 2006) on the basis of the characteristics of the texture. Texture analysis can obtain a better discriminating accuracy. In practical applications, applying which kind of cloud detection algorithm is according to the properties of remote sensing images and the scenarios of applications.

The China-Brazil Earth Resources Satellite program is a technological cooperation program between China and Brazil which develops and operates Earth observation satellites. The third satellite of the series, CBERS-2B (China-Brazil Earth Resources Satellite-2B), was successfully launched on September 19, 2007. In China, CBERS-2B is the first satellite which carried the High Resolution Panchromatic Camera (HRC). The theoretical spatial resolution of this camera is 2.4m. CCD Camera is also on the satellite. And they both work in visible and near infrared bands. The technical parameters of CBERS-2B camera are shown in Table 1.

This paper proposed a discrimination tree which combines the spectrum threshold method and texture analysis method. This structure of the discrimination tree can not only effectively

Received: 2008-06-20; **Accepted**: 2009-02-10

First author biography: Shan Na (1983—), female, Ph.D in Computer Architecture, Institute of Computing Technology, Chinese Academy of Sciences, current research topics: computer architecture, remote sensing image processing research. E-mail: shanna@ict.ac.cn

Table 1 Technical parameters of CBERS-2B camera

	Band	Wavelength/μm	Spatial resolution/m
CCD camera	1	0.45—0.52	19.5
	2	0.52—0.59	19.5
	3	0.63—0.69	19.5
	4	0.77—0.89	19.5
	5	0.51—0.73	19.5
High resolution panchromatic camera	6	0.50—0.80	2.4

distinguish the clouds and objects, but also improve the processing speed. The cloud detection algorithm based upon the structure of the discrimination tree can be widely used to the single-spectral remote sensing image. We also proposed an advanced approach to calculate the fractal dimension value, which can simplify the algorithm and speed up the processing and have no influence on the detection accuracy. The cloud detection algorithm has already been implemented and applied to the image processing system of CBERS-2B.

In this paper, we also investigated how to extend the applications of the cloud detection algorithm. The resources on the remote sensing satellite system are very limited compared with that of the ground system for there are many constraints in technique and conditions in the satellite. So how to make full use of the resources and improve the system performance becomes an important research subject.

2 TRADITIONAL CLOUD DETECTION ALGORITHMS

At present, the most common cloud detection algorithms are based upon the spectral information or the texture information. The spectral analysis distinguishes the clouds and the objects according to the difference of the reflectance and the temperature in the visible and infrared band; texture analysis makes the classification by extracting the spatial statistic feature in the images.

2.1 Spectrum threshold method

The gray value of cloud is much greater than that of objects on the earth, because the cloud has higher reflectivity. This is the basic theory of spectrum threshold method, which was applied to detect the cloud at the very beginning. With the development of multi-spectral sensor, the remote sensing platform can acquire more information. So the detection accuracy can be promoted by extracting the characteristics of cloud and objects in different bands. There are two main ways of choosing the threshold value (Gonzalez & Woods, 2006): analyzing the historical data and extracting information from the image itself. The former may obtain the statistic optimal value, but the information of the image itself is not considered. So it can not guarantee to get the good detection results of every picture. The latter makes good use of the image information, but may encounter the problem of choosing wrong threshold value.

The spectral analysis method is simple and easy to realize. Its high-efficiency characteristic is ideally suited for the large scale data processing in the remote sensing image system. It works well especially under the black background. The large amount of information provided by the multi-spectral sensor enables the algorithm to get more accurate detection results. But the spectrum threshold method is sensitive to threshold value and can be affected by noise. The image data are processed pixel by pixel, leaving the structure information out of consideration.

2.2 Texture analysis

Because the spectral analysis processes the image pixel by pixel and leaves the context information out of consideration, some scholars propose the texture analysis method. The texture feathers of cloud are random and variable, but they are still different from those of the objects on the earth. Texture analysis (Yu *et al*., 2006) is based on spatial frequencies and yields characterizations of textures as smooth, coarse, grainy etcetera. Many natural surfaces such as the coastline and the cloud have a statistical quality of roughness and self-similarity at different scales. This kind of similarity, that the shape of a part is similar to that of the whole, is the most peculiar feature of a shape that have no characteristic length. The fractal and co-occurrence matrix are two good methods of extracting the texture feature from images.

2.2.1 Fractal dimension

Fractal theory (Takayasu, 1990) believes that many things in nature are consistent with certain features, such as self-similarity, fine geometry and so on. Fractal dimension is used to describe the complexity of the fractal. One of the most widely used definitions of the fractal dimension is box-counting dimension (Zhang *et al*., 2005; Li *et al*., 2003).

For the gray-scale image, we can consider the two-dimensional image as a surface (x, y, $f(x, y)$) in three-dimensional space, and $f(x, y)$ is the gray value of the pixel in position (x, y). The variation of gray value reflects the roughness of the surface. The fractal dimension is calculated by using different scales to measure the surface. Firstly, we separate the $M\times M$ image into many $r\times r$ grids in accordance with scale r. On each grid, there are a line of $r\times r\times h$ boxes. Symbol h presents the height of single box, and $h=\lfloor \mathrm{r}\times G/M \rfloor$, where G is the total number of the gray levels. Given the grid (i, j), suppose that the minimum gray value is in box k and the maximum gray value is in box l. The minimum amount of boxes that can cover all the gray values in grid is:

$$n_r(i,j)=l-k+1 \tag{1}$$

Then the amount of boxes that can cover all the images can be calculated by the following formula:

$$N_r=\sum_{i,j} n_r(i,j) \tag{2}$$

Fractal dimension value is:

$$D=\lim \frac{\log(N_r)}{\log(1/r)} \tag{3}$$

We need to define a series of r values, and then draw a scatter diagram with $\log(1/r)$ as abscissa, and $\log(N_r)$ as longitudinal coordinates. By simulating the sample points with least square method, we can get the slope of the line which is the value of the fractal dimension, as shown in Fig. 1.

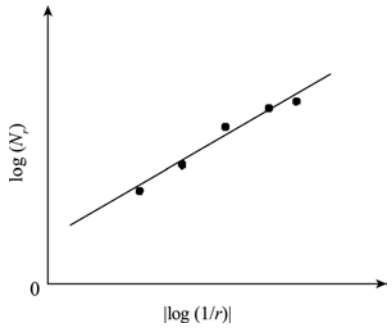

Fig. 1 Fractal dimension D

Fractal dimension value reflects the complexity of the texture feature. The greater the value is, the more complex the fractal is, and vice versa. In the remote sensing images, the ground target has more texture details and its gray value changes obviously, so its fractal dimension value is greater than that of the cloud, for the cloud contains less texture details and its gray value changes smoothly.

2.2.2 Gray level co-occurrence matrix

Gray level co-occurrence matrix is another effective approach of extracting the texture feature (Li, 2006). Gray level co-occurrence matrix reveals certain properties about the spatial distribution of the gray levels in the texture image. The $G\times G$ gray level co-occurrence matrix P for a displacement vector $d = (\Delta x, \Delta y)$ is defined as follows. The entry (i, j) of P is the number of occurrences of the pair of gray levels i and j which are a distance d apart. Formally, it is given as:

$$P(i,j) = \#\{(x_1,y_1),(x_2,y_2) \in M\times N \mid f(x_1,y_1) = i, f(x_2,y_2) = j\} \quad (4)$$

where $\#(x)$ presents the number of the element in set x, P is an $N_g\times N_g$ matrix, $f(x, y)$ is a two-dimension digital image, $M\times N$ is the size of the image, N_g is the gray level.

Haralick has proposed a number of useful texture features that can be computed from the co-occurrence matrix. Angular second moment (energy) is one of them which reflects the regularity of the texture. It is defined as follows:

$$\mathrm{ASM} = \sum_i \sum_j [p(i,j)]^2 \quad (5)$$

where $p(i, j)$ is the value of entry (i, j) in normalized gray level co-occurrence matrix.

The coarse texture contains more energy, its angular second moment value is greater, and vice versa. According to this theory, clouds have greater value of angular second moment than ground objects.

Texture analysis approach requires plentiful sample data to get the characteristics of different subjects. The quantity and quality of the samples directly influence the accuracy of the algorithm.

3 CLOUD DETECTION ALGORITHM BASED ON TEH DISCRIMINATION TREE

As Section 2 describes, the spectrum threshold method and the texture analysis method can get the satisfied results under certain situation, but they both have disadvantages. The spectrum threshold method makes full use of the characteristic of reflectivity, but processes the image pixel by pixel, leaving the spatial context information out of consideration. While the texture analysis method analyzes the relationship between pixels, extracts the features of the surface in terms of roughness, similarity and so on, but it ignores the particular spectral features.

High Resolution Panchromatic Camera (HRC) and CCD Camera carried on the CBERS-2B satellite are both work in visible and near infrared bands. So the multi-spectral threshold approach is not suitable. A recent study (Luis *et al*., 2006) shows that the cloud detection result in near infrared bands is much better than in visible bands. Therefore, B4 band (wavelength: 0.77—0.89μm) is most expected band in the process of detection, and B3 band (wavelength: 0.63—0.69μm) and B5 band (wavelength: 0.51—0.73μm) are preferred, too.

3.1 Feature values

To process fast, optimizations are required. In this section, we discuss how to select the feature parameters and extract them. And we also elaborate an advanced fractal dimension computing method.

3.1.1 Threshold

The threshold value is a key parameter, which severely affects the accuracy of the detection. We extract the threshold value from the historical image data. Because this approach does not require the other information and the threshold value will get closer to the optimal value as the data increase. We choose 169943040 sample pixels of the remote sensing images acquired by CBERS-2B to evaluate the threshold value. There are approximate 95% sample points whose gray values are between 200 and 255, so we select 200 as the threshold value.

Traditional spectrum threshold method processes the images pixel by pixel, but texture analysis method processes the images by $N\times N$ sub-image. So some modifications should be made to unify the processing unit. In this case, the concept of cloud threshold percent is put forward that presents the percentage of the cloud pixels in an $N\times N$ sub-image. According to the cloud threshold percentage, the algorithm classifies the sub-image into different categories. The critical value is estimated by training the sample data.

3.1.2 Advanced fractal dimension method

Calculating the fractal dimension value is a time-consuming

and computing-intensive task (Ding *et al*., 2006). The procedure contains several traversals of image data and large amount of complicated calculating operations. In order to improve the efficiency, we optimize the procedure of calculating the fractal dimension by recording the intermediate results and simplifying the formula.

Texture analysis processes the image by 64×64 sub-images. The scale factor r is of great importance for the accuracy of the results. If the scale factor r is too small, the results will be too sensitive to the noise; on the other hand if it is too big, it will be hard to extract the texture characteristics. Thinking over the size of sub-image and the texture feature to be extracted, the scale factor r is defined as 4, 8 and 16. There are certain spatial relationships between the divided data sub-blocks, shown as Fig. 2. The maximum and minimum value in scale 8 data sub-block must be one of the maximum and minimum values in scale 4 data sub-block in the same position. The relationship between scale 16 and scale 8 is the same. So we can accomplish the calculation just through once traversal of the image by recording the intermediate results. Firstly, we divide the image in scale 4, and find the maximum and minimum value of each sub-block. Then we record the maximum and minimum value in form of intermediate results. When processing the scale 8 sub-blocks, we search the intermediate results instead of the original image to find the maximum and minimum value. The same approach applies to scale 16. This method obviously reduces the traversal and the comparison operation, and improves the efficiency of the algorithm.

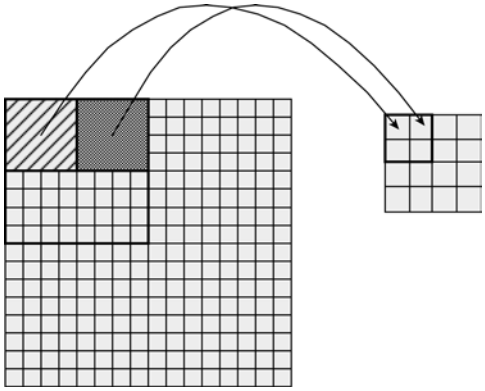

Fig. 2 The spatial relationship of scale factor 4, 8 and 16

Because the procedure computing $\log(1/r)$, $\log(N_r)$ and simulating the sample points with least square method contains multiplicaton, division and log operations, the operations are complex and time-consuming for hardware implementation. By expanding and simplifying the formula we can redefine the formula of the fractal dimension as follows:

$$D = (\log_2^{N_{r4}} - \log_2^{N_{r16}})/2 \quad (6)$$

(* Division operation can be replaced by shift operation)

N_{r8} disappeared in the new formula, so we do not need to perform box-counting operation in scale 8. The pseudo-code of the algorithm is as follows:

```
Algorithm CAL_D (){
    for (i=0; i<image_height; i+=4) {
       for (j=0; j<image_width; j+=4) {        //scale r=4, computing nr
            Find max and min value;
            Save the max and min value;     //save the intermediate results
            Compute nr4;
        }
    }
    for (i=0; i< image_height/4; i+=2) {
         for (j=0; j< image_width/4; j+=2) {     //scale r=16, computing nr
              Find max and min value;
              Compute nr16;
         }
   }
    Compute and return D_value;
}
```

Since the characteristics of images acquired by different sensors and in different bands are quit differently, we need to train the image data separately. We choose 41490 cloud sub-images and 31950 object sub-images as the samples. The training results are shown in Fig. 3 and Fig. 4.

The fractal dimension values of cloud sub-images are lumped. About 43% fractal dimension values are 2.0, and 98% are between 1.9534 and 2.4500. In contrast, the fractal dimension values of object sub-images are dispersive. The values evenly distribute within the range between 1.8 and 2.3. The training results indicate that if the fractal dimension values are in range of 1.9534 and 2.4500, the possibility for cloud is great. But it can not distinguish the cloud and object very clearly. In practice, the range of the fractal dimension value changes as the image data acquired by satellite increase.

3.1.3 Angular Second moment

The angular second moment also needs plenty of samples to be trained to obtain the distributed space. We use the same samples as training the fractal dimension value. The results are shown in Fig. 5 and Fig. 6.

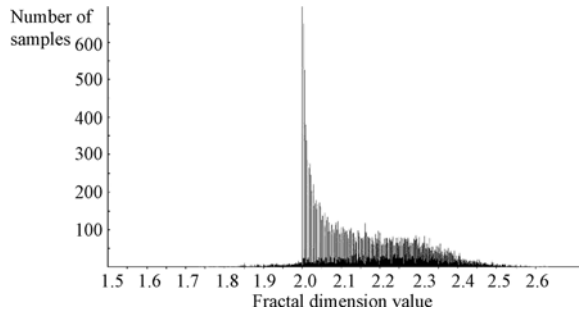

Fig. 3 The distribution of the fractal dimension value of cloud
The fractal dimension value in abscissa 2.0 is far beyond the confine of presentation

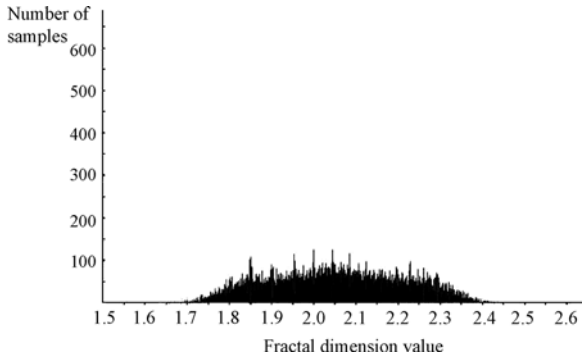

Fig. 4 The distribution of the fractal dimension value of ground-objects

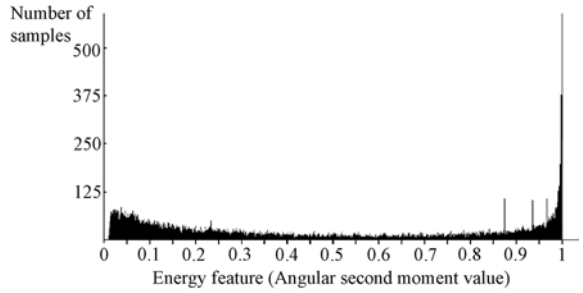

Fig. 5 The distribution of the energy feature of cloud
The angular second moment value in abscissa 1.0 is far beyond the confine of presentation

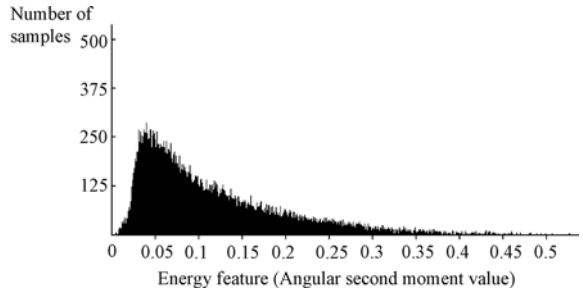

Fig. 6 The distribution of the energy feature of ground-objects

The angular second moment values of cloud sub-images are relatively concentrated. About 38% angular second moment values are 1.0, and more than 50% are between 0.9150 and 1.0000. The angular second moment values of object sub-images are mainly distributed between 0.0365 and 0.2584. The training results shown in Fig. 5 and Fig. 6 indicate the angular second moment values can be used to effectively distinguish the cloud and object. In practice, the range of the angular second moment values changes as the image data acquired by satellite increase.

3.2 New algorithm based on the structure of the discrimination tree

How to use these two methods described above properly has a great impact on the detection accuracy. Gray value is a key parameter which is used to distinguish the cloud and cloud-free pixels roughly. It is helpful to begin with a rough and ready classification. But the noise and the snow can not be separated from the cloud by the gray value. This will decrease the accuracy. These misjudged-pixels are able to be excluded by the space context because the texture features of clouds and objects are quite different. So the texture analysis approach can make the accurate classification. The fractal dimension and the angular second moment are two texture feature parameters describing the image texture characteristics from different aspects. The fractal module focuses on the self-similarities of irregular images and is adequate for classification, while the angular second moment measures the uniformity of the distribution of gray level and is suitable to distinguish the congener objects. The structure of the discrimination tree is proposed to take the advantage of these parameters. Fig. 7 shows the structure of the discrimination tree.

According to the structure of the discrimination tree, the sub-images are classified into three categories: cloud-like (probably is cloud), object and ambiguous (may be cloud, may be object). Different categories will take different processing procedure. The sub-images in object group have accomplished the classification. The sub-images in cloud-like group need to be reconfirmed by the texture feature. If the fractal dimension value is in the range of the cloud, then the sub-image is determined to be cloud. Otherwise, the angular second moment will be calculated to make sure the sub-image not be misjudged (missed detection). The same approach can be used in ambiguous group. The angular second moment is used to reduce the false alarming rate. By using the structure of the discrimination tree we can not only promote the detection accuracy but also improve the average efficiency of the algorithm, since there is no need to calculate all the parameters of the features to accomplish the classification in the whole procedure. In the discrimination tree, the leaf node is the result of the detection. So the calculations of fractal dimension and angular second moment which are intensive computing and time-consuming tasks can be omitted in some cases. This structure is very suitable for the large-scale images processing scenario.

4 EXPERIMENTAL RESULTS ANALYSIS AND ALGORITHM APPLICATION

In this section, results from testing the cloud detection al-

gorithm are presented. We use the real gray-scale image data acquired by CBERS-2B. The algorithm performance and detection accuracy are analyzed and discussed.

4.1 Performance

The advanced fractal dimension procedure and the structure of the discrimination tree proposed in this paper can obviously improve the efficiency of the cloud detection algorithm. The advanced fractal dimension procedure reduces image traversals and complex computing operations. And the structure of the discrimination tree speeds up the average running time.

4.1.1 The advanced fractal dimension procedure

The improvements of performance brought by the advanced fractal dimension procedure are mainly manifested in two aspects: on the one hand, the advanced fractal dimension procedure takes advantage of spatial location of different scales to reduce the image traversals by saving the intermediate results, which avoids frequent memory access; on the other hand, the advanced fractal dimension procedure simplifies the equation, which eliminates a lot of complex operations. The comparison of the original method and advanced method is shown in Table 2. All the summarized values are based on the 64×64 sub-image.

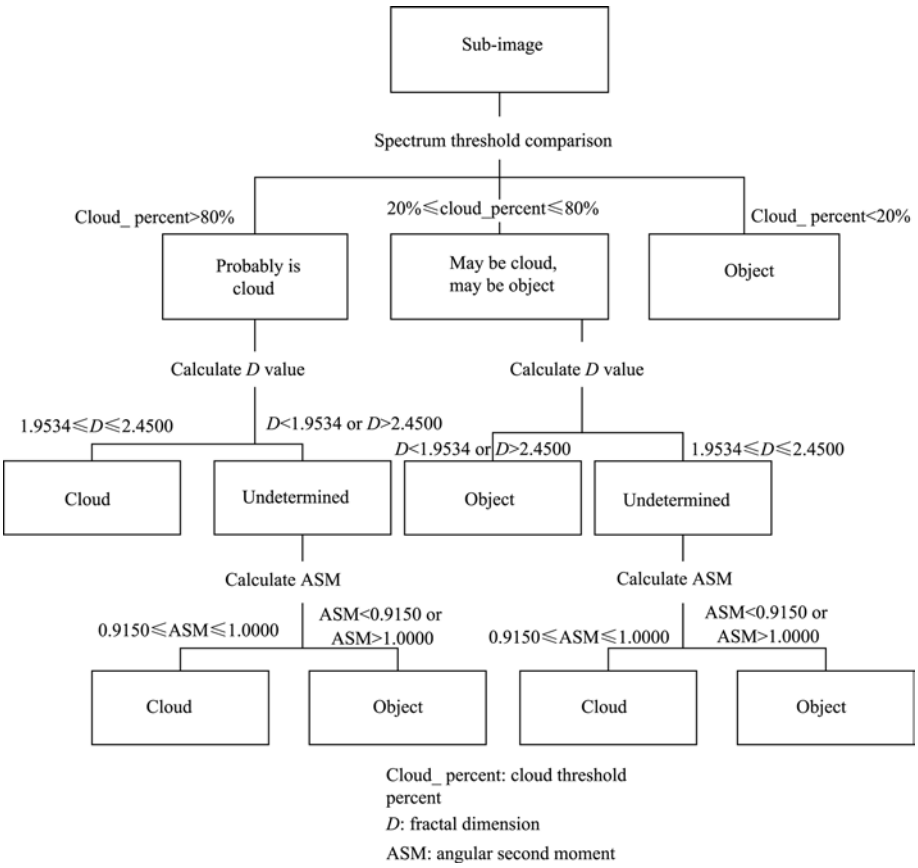

Fig. 7 The structure of the discrimination tree of the cloud detection algorithm

Table 2 Comparison between advanced fractal dimension algorithm and fractal dimension algorithm

	Traversal Times	Log operation	Multiply operation	Divide operation	Comparison operation
Original method	3	18	10	1	23904
Advanced method	1	2	0	0#	8160

Division operation can be replaced by shift operation.

From Table 2, we can see that image traversals reduced from 3 to 1, and the complex operations reduced by two-thirds at least. Meanwhile, the software program has been optimized which promoted the efficiency further. We select 42120 sub-images in size of 64×64, whose total volume is 165MB, and verify the algorithm in personal computer. The hardware configuration of the computer is as follows: a Pentium 4 3.06GHz CPU, DDR2 800MHz 1.50GB memories and an 80GB hard disk. The time consumed by different algorithm is shown in Table 3.

Table 3 Efficiency comparison between advanced fractal dimension algorithm and fractal dimension algorithm

	Processing time/s
Original method	18.463
Advanced method	3.313

The errors of the original method mainly come from the calculation error of the least square method. The advanced algorithm just makes use of the spatial location of different scales and simplifies the formulation. Therefore, there is no change in the accuracy of advanced method compared with the original method.

4.1.2 The structure of the discrimination tree

By using the structure of the discrimination tree we could obtain the detection results without calculating all the parameters. So the structure of the discrimination tree can improve the average performance of the algorithm.

The execution path is closely related to the cloud coverage of the image. We select three typical images: almost all the clouds, almost clouds free and partly clouds. Each category picks 6 images in size of 6132×5812. Under the same test environment, each image is processed by the algorithm using the structure of discrimination tree and the algorithm not using the structure of discrimination tree respectively. Table 4 recorded the average testing results.

Table 4 Running time of this two discrimination structure

	Using the structure of the discrimination tree/s	Not using the structure of the discrimination tree/s
Almost clouds free	0.224	2.365
Almost all the clouds	0.794	2.254
Partly clouds	0.972	2.431

From these results we can see that the structure of the discrimination tree improves the average performance of the algorithm, especially in the case of almost clouds and almost clouds free. The processing time shortens more than ten times at best. For the image partly covered by clouds, the algorithm efficiency is promoted too.

4.2 Accuracy

We process the real remote sensing images acquired by the China-Brazil Earth Resources Satellite-2B using the cloud detection algorithm proposed in this paper. The results output the cloud coverage of the image (the image is divided into four parts: top left, top right, bottom left and bottom right) and the cloud extracting images. The two critical evaluation criterions of the accuracy of the algorithm are the false alarming rate (misidentified the object as the cloud) and the missed detection rate (misidentified the cloud as the object). The experimental results illustrate that the false alarming rate is less than 5% and the missed detection rate is less than 10%. Fig. 8(a) and Fig. 9(a) show the original remote sensing images. And the detection results are shown in Table 5.

Fig. 8(b) and Fig. 9(b) show the cloud extraction images.

Table 5 Cover rate result of the cloud detection

	Top left/%	Top right/%	Bottom left/%	Bottom right/%
Fig. 8(a)	37.15	99.58	55.26	84.69
Fig. 9(a)	83.26	88.39	14.35	3.84

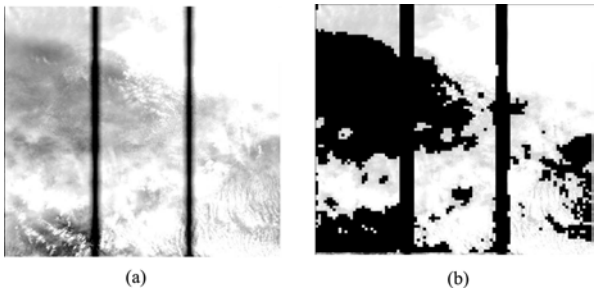

Fig. 8 Plain area image data acquired by CBERS-2B
(a) Original image; (b) Extract image of cloud

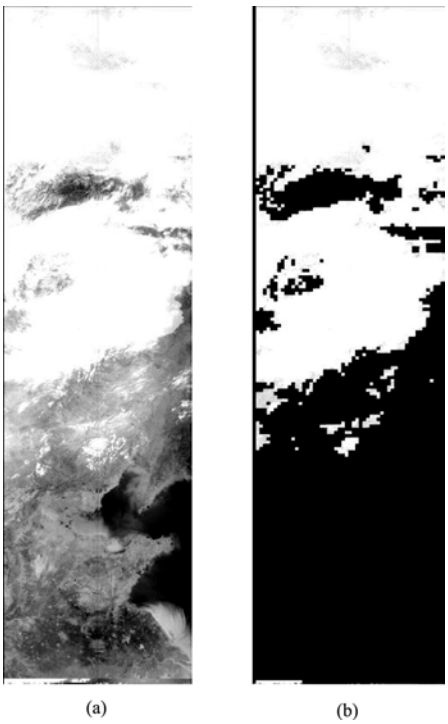

Fig. 9 Mountain area image data acquired by CBERS-2B
(a) Original image; (b) Extract image of cloud

The cloud detection algorithm is of high universality for the optical remote sensing images. In order to prove it, we verify the algorithm with new remote sensing images which acquired by another satellite working in visible and near infrared bands. The raw images are shown in Fig. 10 (a) and Fig. 11(a) and the cloud coverage results calculated by the algorithm are presented in Table 6. The cloud extraction images are shown in Fig. 10(b) and Fig. 11(b).

Table 6 Cover rate result of the cloud detection

	Top left/%	Top right/%	Bottom left/%	Bottom right/%
Fig. 10(a)	31.50	90.29	66.17	85.13
Fig. 11(a)	13.11	77.46	95.91	97.57

In most cases, the cloud detection algorithm classifies the clouds and the objects efficiently and accurately. But the false detection and missed detection still exist. The false detection is mainly caused by the snow, because the spectral feature and the texture feature of snow are strikingly similar to those of clouds.

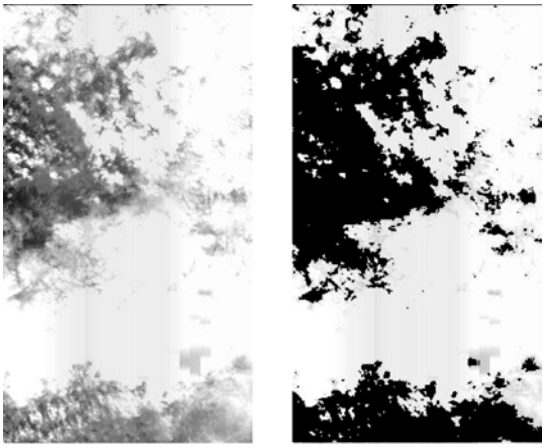

Fig. 10 Plateau area image data acquired by optical remote sensing satellite α
(a) Original image; (b) Extract image of cloud

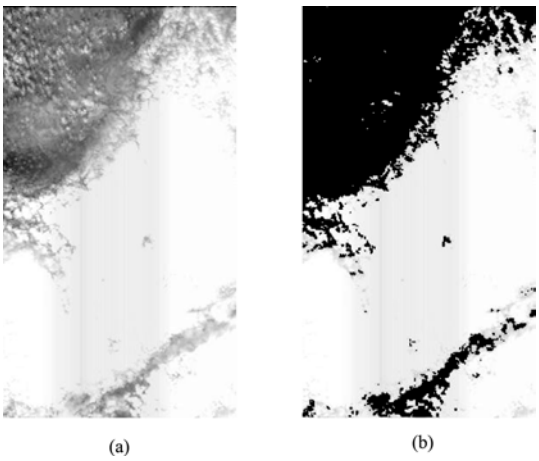

Fig. 11 Plain area image data acquired by optical remote sensing satellite α
(a) Original image; (b) Extract image of cloud

The missed detection mainly results from cloud edges. The cloud edges change sharply and have more details which were more like the feature of the objects on the earth. These problems are the places which need to be studied and improved.

At the present day, the cloud detection results are mainly used to discard the "useless" images, or evaluate the remote sensing image quality. The potential information is not utilized effectively. On the other hand, the resources of remote sensing system are expensive and limited. So how to make full use of the information to improve the utilization and performance of the system is becoming the hot research topic in this field.

Selective compressing or discarding data is a form of dynamic scheduling, which can save the storage and downlink resources. It is an effective policy to increase resource utilization rate and improve the system performance. Another excellent policy is cloud cover avoidance mechanism, which formulated by effectively predicting the cloud cover situation (Algra, 2002). The prediction is based on the cloud information associated with the digital climate models or the historical meteorological data. There are two cloud cover avoidance methods: selective imaging and cloud editing. Selective imaging means that the remote sensor only records the parts of cloudlessness area by the prediction; cloud editing is a process implying that parts of the image data that are cloud covered are discarded, or represented in only one band or represented at a lower resolution. Additionally, if the cloud sensing provides the ability to point the optical axis of the satellite remote sensing instrument to cloud-free areas on the basis of previously acquiring cloud cover information (Algra, 2003), the effective imaging capacity of the mission can be remarkably improved.

5 CONCLUSIONS

This paper introduced in detail the fundamental principle of the spectrum threshold method and texture analysis method, and further in-depth studied the influence on detection accuracy of different criterions. We proposed an advanced fractal dimension computational method which can enhance the performance with no impact on the accuracy. We also proposed a structure of the discrimination tree which defined how to use the criterion properly. The cloud detection algorithm has been implemented by software, and verified using the real remote sensing data. The results illustrate the good performance and high detection accuracy. We also investigated the potential application of the cloud detection algorithm.

Acknowledgements: This project is supported by China Center for Resources Satellite Data and Applications and Institute of Computing Technology, Chinese Academy of Sciences.

REFERENCES

Ding B H, Li W C and Wang F M. 1999. Analysis of fractal image and design of fractal dimension calculation program. *Journal of University of Science Technology Beijing*, **21** (3): 304—307

Gonzalez R C and Woods R E. 2006. Digital Image Processing. Beijing: Publishing House of Electronic Industry

Li B C. 2006. Texture feature retrieval and applications using gray co-occurrence matrices. *Journal of Kashgar Teachers College*, **27** (6): 35—37

Li M, Liew S C and Kwoh L K.2003. Producing cloud free and cloud-shadow free mosaic from cloudy IKONOS images. Geoscience and Remote Sensing Symposium Proceedings

Li Y C, Sun H, Xu M and Zhang X H. 2003. Box-counting method and its application to the detection of fog using GMS-5 weather satellite data. *Bulletin of Sciences and Technology*, **19** (1): 29—31

Liu Z G, Li Y X and Huang F. 2007. Cloud detection of MODIS satellite images based on dynamical cluster. *Remote Sending Information*, **4**: 33—35

Loyola D. 1998. A new cloud recognition algorithm for optical sensors.

Geoscience and Remote Sensing Symposium Proceedings

Luis G C, Gustavo C V, Julia A, Jose D M, Javier C, Luis A, Luis G, Juan C F and Jose M. 2006. Cloud detection for MERIS multis-pectral images. Geoscience and Remote Sensing Symposium Proceedings

Song X N and Zhao Y S. 2003. Cloud detection and analysis of MODIS image. *Journal of Image and Graphics*, **8** (9): 1079—1083

Takayasu H. 1990. Fractals in The Physical Sciences. Manchester: Manchester University Press

Theo Algra. 2002. On the effectiveness of cloud cover avoidance methods in support of the supper-spectral mission for land applications. Geoscience and Remote Sensing Symposium Proceedings

Theo Algra. 2003. Real-time cloud sensing for efficiency improvement of optical high-resolution satellite remote sensing. Geoscience and Remote Sensing Symposium Proceedings

Wang R F, Sun L, Zhang J and Song P J. 2006. The application analysis of spectrum threshold and MSC cloud detection algorithms based on “HY-1A” CCD data. *Acta Oceanologica Sinica*, **28** (6): 158—163

Yu W X, Cao X G, Xu L and Mohamed B. 2006. Automatic cloud detection for remote sensing image. *Chinese Journal of Scientific Instrument*, **27** (6): 2184—2186

Zhang Z, Dong F A and Wu Y L. 2005. Estimation of fractal dimension for 2-D gray image. *Computer Applications*, **25** (12): 2853—2854

快速高准确度云检测算法及其应用

单　娜[1,2], 郑天垚[1], 王贞松[1]

1.中国科学院 计算技术研究所, 北京　100190;
2. 中国科学院 研究生院, 北京　100190

摘　要: 采用光谱阈值判别和纹理分析相结合的方法, 提出一种基于树状判别结构的快速高准确度云检测算法, 综合利用多个判别准则, 确定图像中云层覆盖情况, 与传统方法相比能够获得更高的分辨精确度。树状判别结构还能够在平均意义上显著提高算法运行效率。同时, 提出了一种改进的分形维数计算方法, 能够在不影响精确度的前提下, 使算法的运行效率提高 5 倍左右, 基本满足实时性的要求。所提出的云检测算法已在中巴地球资源卫星项目中实际应用, 实际测试结果表明, 该算法达到自动云检测的虚警概率小于 5%, 漏警概率小于 10%的工程要求。

关键词: 遥感卫星图像, 云层检测, 分形维数计算, 灰度共生矩阵, 树状判别结构

中图分类号: TP751.1　　文献标识码: A

1 引　言

应用卫星遥感技术获取地球表面物体的遥感图像, 为气象观察预测、地球资源普查、环境污染检测和自然灾害监测等领域提供了丰富的遥感信息。在遥感成像过程中, 由于受大气密度、天气变化等影响, 许多卫星遥感图像存在云层遮挡的“盲区”, 局部地物信息丢失, 不利于图像的分析与解释。因此实时有效的进行云层检测, 剔除云覆盖率大的图像, 对于缓解遥感图像海量数据对传输通道的压力和提高卫星遥感图像利用率有着非常重要的意义。云的种类繁多, 纹理呈现随机分布特性, 其特点受地理位置、季节和气候等多种条件的综合影响, 使得云检测一直以来是遥感图像处理中很难解决的问题。云检测方法众多。早期的方法根据在可见光波段云比大多数地面目标物体有更高的反射率的光谱辐射特性, 通过光谱阈值判别将云和地面物体大致分开。目前已有许多学者在阈值判断方法的基础上研究了更加精确的云检测算法, 如同态滤波法(Li 等, 2003)、统计分析法、聚类法(刘志刚等, 2007; 王瑞富等, 2006)、多光谱分析法(Loyola, 1998; 宋小宁 & 赵英时, 2003)等; 还有学者从纹理特征的角度提出了纹理分析的方法(郁文霞等, 2006), 获得了较好的判别精确度。实际应用中根据遥感图像数据的特点和应用场景等综合决定选择使用哪种检测算法。

2007-09-19 发射成功的中巴地球资源 02B 卫星(CBERS 02B)是中国和巴西合作研制的, 首次搭载了高分辨率相机(high resolution camera, HRC), 理论上分辨率能达到 2.4m, 是目前中国民用领域分辨率最高的卫星。中巴地球资源卫星 02B 的成功发射在民用领域意义重大。CBERS 02B 的高分辨率相机和多光谱 CCD 相机, 工作在可见光和近红外波段, 具体参数见表 1。

针对 CBERS 02B 遥感卫星图像数据主要为可见光/近红外波段数据的特点, 将光谱阈值判断法和纹理分析方法结合起来, 提出了一种树状判别结构。利用这种树状判别结构, 不仅能够有效的区分云区和下垫面, 获得较高的分辨精确度, 还能够在平均意义上显著提高算法运行效率。

表 1　CBERS 02B 相机技术参数

	波段号	波长/μm	地面分辨率/m
CCD 相机	1	0.45—0.52	19.5
	2	0.52—0.59	19.5
	3	0.63—0.69	19.5
	4	0.77—0.89	19.5
	5	0.51—0.73	19.5
高分辨率相机	6	0.50—0.80	2.4

收稿日期: 2008-06-20; 修订日期: 2009-02-10

第一作者简介: 单娜(1983—　), 女, 中国科学院计算技术研究所, 计算机系统结构方向, 在读博士生, 现主要从事计算机系统结构设计及遥感图像处理方面的研究。E-mail: Shanna@ict.ac.cn。

2 传统遥感图像云层检测算法

目前，最常用的云检测算法是利用遥感图像的光谱信息或纹理信息进行云与地面物体的区分。光谱分析利用云与地面物体在可见光和红外波段的反射率和温度的差异进行分辨；纹理分析利用物体的局部或整体有着某种程度的自相似性，通过提取目标物体的空间统计特性，将各类目标物体归类。

2.1 基于图像光谱阈值进行判别

云在可见光/近红外波段对于光线的反射率比大多数地面物体要强得多，在卫星遥感图像上表现为相对于地面目标有较高的灰度值。利用云的这个特性，可以使用阈值判断方法对卫星遥感图像进行粗略的云与地面物体的判别。这是最早的云层检测使用的方法。随着多光谱传感器的出现和发展，通过遥感平台能够获得更丰富的遥感图像信息。提取云和地面物体在不同波段的特征差别，形成多维特征向量，能够更加精确的进行云检测。图像光谱阈值的确定(Gonzalez & Woods, 2006)大致有两种方法：一是根据经验，通过对数据库中大量的历史样图进行统计，获取云层的经验阈值；二是利用图像本身的信息，确定阈值的选取。经验阈值的方法可以在统计意义上接近最优，但是没有考虑图像本身的信息特点，所以不能保证对每幅遥感图像得到很好的分辨结果。利用图像自身信息的方法，虽然充分利用了图像自身数据特点，却可能会遇到无法正确选取阈值的问题。

光谱分析方法简单，易实现，执行效率高，非常适合遥感图像数据量大的特点，对于黑色背景下的云有着很好的分辨效果。多光谱丰富的数据信息使光谱分析法能够获得更精确的判别结果。光谱分析存在的问题是对阈值比较敏感，阈值的选择有一定的主观性，精确度容易受噪声的影响。同时，光谱分析以像元为处理的基本单位，没有考虑图像的结构信息。

2.2 基于云的纹理特征分析

针对光谱阈值法中点与点之间的独立处理，忽略像元间空间上下文信息的缺陷，有学者提出了基于纹理分析的云层检测方法。虽然云的纹理基元多变难测，属于随机纹理，但它仍有别于下垫面物体的纹理特征。基于云层纹理特征的分析利用云的局部和整体有着某种程度的相似性，从图像的统计特征出发，提取云与地球表面物体的纹理特征，对云和地球表面物体进行有效的区分(郁文霞等, 2006)。云检测算法中最常用的纹理特征有分形维数和角二阶矩值。

2.2.1 基于分形维数进行判别

分形理论认为，自然界中的许多事物具有某些一致性的特征，如自相似性、精细的几何结构等等(Takayasu, 1990)。分形理论通过分形维数的概念反映分形的复杂程度。计盒维数是应用最为广泛的分形维数定义之一(张志等, 2005; 李亚春等, 2003)。

对于灰度图像而言，把二维图像视作三维空间中的一个表面(x, y, $f(x, y)$)，其中 $f(x, y)$为图像(x, y)位置处的灰度值，图像灰度的变化情况将反映该表面的粗糙程度。使用不同尺度度量该表面，计算得到的维数就是图像的分形维数。将 $M\times M$ 大小的图像按照尺度 r 分割成许多 $r\times r$ 的网格。在每个网格上，是一列 $r\times r\times h$ 的盒子，单个盒子的高度 $h=\lfloor \mathrm{r}\times G/M \rfloor$，其中 G 为总的灰度级数。设在第(i, j)网格中图像灰度的最小值和最大值分别落在第 k 和第 l 个盒子中，则覆盖第(i, j)网格中的图像灰度值所需的盒子数为:

$$n_r(i, j)=l-k+1 \tag{1}$$

进而求出覆盖整个图像所需的盒子数为:

$$N_r=\sum_{i,j} n_r(i, j) \tag{2}$$

分形维数值为:

$$D=\lim \frac{\log(N_r)}{\log(1/r)} \tag{3}$$

选取一组 r，以 $\log(1/r)$为横坐标，$\log(N_r)$为纵坐标绘制点聚图。利用最小二乘法拟合样本点，所得的斜率即为此图像样本的分形维数 D，如图 1。

分形维数值反映物体纹理的复杂程度。分形维数值越大，表明分形越复杂，反之则表明分形越规则。遥感图像中地面目标物体灰度值变化明显，纹理细节丰富，其分形维数值偏大；云层灰度值变化平缓，纹理细节少，其分形维数值偏小。

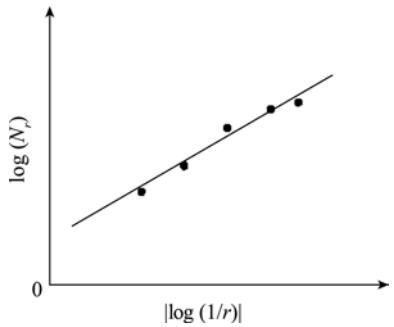

图 1 分形维数 D

2.2.2　基于灰度共生矩阵进行判别

灰度共生矩阵是纹理特征提取的另一种有效方法(李丙春, 2006)。灰度共生矩阵实际上是描述一个两维数字图像中等灰度的面积(归一化后的)大小的分布情况。共生矩阵用两个位置的像元的联合概率密度来定义。位于矩阵中(i, j)位置的元素$P(i, j)$表示一个灰度为i而另一个灰度为j的两个相距为$(\Delta x, \Delta y)$的像元对出现的次数。

$$P(i,j)=\#\{(x_1,y_1),(x_2,y_2)\in M\times N \mid f(x_1,y_1)=i, f(x_2,y_2)=j\} \quad (4)$$

其中$\#(x)$表示集合x中的元素个数，P为$N_g\times N_g$的矩阵, $f(x, y)$为一幅二维数字图像, $M\times N$为图像大小, N_g为灰度级。

作为图像纹理分析的特征量是由灰度共生矩阵计算出的一些参量。其中，角二阶矩(能量)反映纹理均一规则性。角二阶矩值的计算如公式(5)。

$$\mathrm{ASM}=\sum_i\sum_j[p(i,j)]^2 \quad (5)$$

公式中$p(i, j)$是归一化灰度共生矩阵中位置(i, j)处元素的值。

从图像整体观察，纹理较粗，其 ASM 值较大，含有的能量较多；反之，细纹理，其 ASM 值较小。云层纹理粗，其 ASM 值较大，所含能量多；地面目标物体纹理细，其 ASM 值较小，所含能量小。

纹理分析方法要求足够的样本数据进行训练以得到不同类别物体的特征值区间，样本质量和数量直接影响训练区间的准确性，继而影响算法的判别精确度。

3　基于树状判别结构的云检测算法

基于图像光谱阈值判别方法和基于图像纹理分析的判别方法对于某些特定的图像能获得比较满意的结果，但存在不可避免的缺陷。光谱阈值判别法充分利用了物体的反射特性，但点与点之间的处理相互独立，忽略了图像像元之间的空间上下文信息; 纹理分析的方法从统计的角度，分析像元点之间在空间上的相互关系，提取物体表面纹理的粗糙程度、变化规律和相似程度等特征，但忽视了云的独特光谱特征。

CBERS 02B 搭载的高分辨率相机和 CCD 相机工作在可见光/近红外波段，因此无法使用多光谱阈值判别方法。越接近红外波段云检测的效果越好(Luis 等, 2006)，因此 CBERS 02B 的波段 4(波长: 0.77—0.89μm)最适合进行云层检测，波段 3(波长: 0.63—0.69μm)和波段 5(波长: 0.51—0.73μm)也可获得较好的检测结果。

3.1　特征选择及提取

新算法的有效实施需要对特征参数的传统定义作适当修改。

3.1.1　阈值

阈值是影响光谱分析精确度的关键因素。两种常用的阈值确定方法在实际中有广泛应用，由于云检测算法需要满足实时性要求，尽可能的减少计算量成为选择算法时考虑重要因素。经验阈值法虽然无法充分利用图像自身的信息，但是使用经验阈值不需要对图像进行额外处理，计算量小，并能确保图像不会因为无法正确选择阈值导致无法处理。随着遥感系统不断采集图像数据，样本数量增加，经验阈值可以不断优化，最终达到一个理想的阈值点。通过对中巴资源卫星获取的 169943040 个典型云层样本点进行统计，95%的样本点其像元灰度值在 200—255 之间，因此选择 200 作为经验光谱阈值。

传统光谱阈值法以像元为处理单元，而纹理分析方法以子图为处理单元，为使算法前后处理单元基本一致，对传统光谱阈值法做相应的调整。本文以子图图像为处理单元，提出阈值百分比的概念，即待处理子图中灰度值大于阈值的像元点所占百分比。根据阈值百分比值将子图划分为不同类别。临界值的确定通过大量的实验样本训练得到。

3.1.2　分形维数计算的快速算法

传统的分形维数计算方法需要对子图进行多次遍历，每次遍历包含大量复杂运算，导致算法运行效率低(丁保华等, 2006)。为了提高算法效率，我们提出一种改进的分形维数计算方法。

纹理分析通常选取 64×64 大小的子图作为基本的处理单元。在计算分形维数时，尺度因子的选择非常重要，尺度因子过小会受到噪声的严重影响，而尺度因子过大则会难以提取纹理特征。综合考虑子图大小和待提取物体类别的纹理特征，结合图像像元点的空间分布关系，选择 4、8、16 三个尺度因子。由 3 个尺度因子划分的子块数据之间存在空间位置上的包含关系，如图 2。利用这种空间包含关系，可以实现一次图像遍历，完成分形维数的计算。先以尺度因子 4 划分子图，形成一系列网格，确定覆盖网格的盒子数时，将该网格中的图像灰度最大值和最小值以中间结果的形式保存下来。在以尺度 8 划分子图，计算覆盖每个网格的盒子数时，直接从

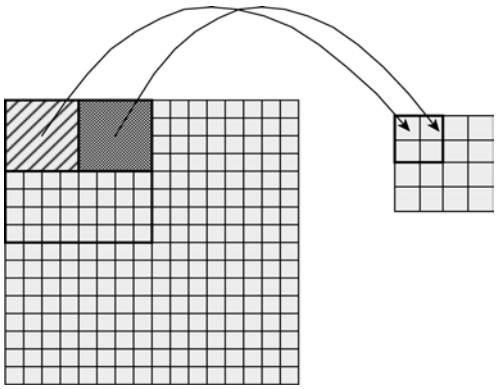

图 2 4、8、16 尺度因子的空间关系

保存的中间结果中查找对应的灰度最大最小值。同样的方法应用于计算尺度因子为 16 的子块数据。使用这种方法不仅减少图像的遍历次数，并且显著减少了像元灰度值的比较操作，能够明显提高算法的执行速度。

得到 3 个尺度因子对应的 N_r 值，即可利用最小二乘法拟合 $\log(1/r)$、$\log(N_r)$。该计算过程中用到了乘法、除法及对数等复杂运算操作。将最小二乘法拟合公式展开，通过换底公式将对数运算换成以 2 为底数，对公式进行化简，得公式(6):

$$D=(\log_2^{N_r 4}-\log_2^{N_r 16})/2 \quad (*除法用移位操作实现) \tag{6}$$

化简抵消了带有尺度因子 8 的计算项，可以直接省略计算尺度因子为 8 的计盒操作，由尺度因子 4 的中间结果直接生成尺度 16 的结果。算法的具体实现如下:

```
algorithm CAL_D(){
    for(i=0;i<image_height;i+=4){
        for(j=0;j<image_width;j+=4){
        //计算尺度 r=4 时的 nr
            find max and min value ;
            save the max and min value;
            //保存中间结果
            compute nr4;
        }
    }
    for(i=0;i< image_height/4;i+=2){
        for(j=0;j< image_width/4;j+=2){
        //计算尺度 r=16 时的 nr
            find max and min value ;
            compute nr16;
        }
    }
    compute and return D_value;
}
```

不同传感器获取的不同波段的遥感图像特点不同，需要针对不同类型的遥感图像单独训练，增加检测的准确性。我们从中巴资源卫星获取的遥感图像数据中选取了 41490 个云层子图图像样本和 31950 个下垫面子图图像样本，训练结果如图 3、图 4。

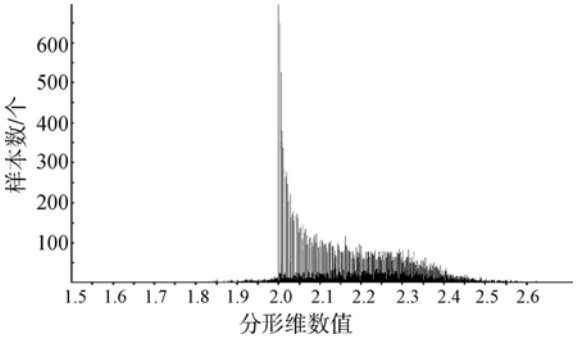

图 3 云层子图的分形维数值分布
(横坐标 2.0 处的分形维数值远超出其坐标所表示的范围)

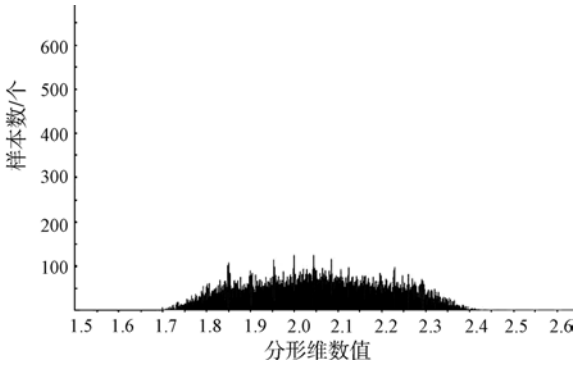

图 4 下垫面子图的分形维数值分布

云层子图的分形维数值非常集中，样本图像中有 43%的样本分形维数值为 2.0，98%的样本分形维数值在 1.9534—2.4500 之间。下垫面子图的分形维数值则相对分散很多，样本图像的分形维数值主要分布在 1.8—2.3 之间，且分布较为均匀。从训练结果看，分形判别方法对云的判别的肯定性极高，但是对云与下垫面的区分性不太高。在实际的应用中，随着遥感平台不断获取真实遥感图像样本数据，云层及下垫面的分形维数分布区间边界值将根据训练结果进行调整。

3.1.3 角二阶矩值

角二阶矩值也需要对大量的云层样本图像和下垫面样本图像进行训练，得到云和下垫面角二阶矩值的分布空间。选择与训练分形维数值相同的图像样本进行角二阶矩值的测试，结果如图 5、图 6。

云层子图的角二阶矩值相对比较集中，样本图像中有 38%的样本角二阶矩值为 1.0，50%以上的样本角二阶矩值在 0.9150—1.0000 之间。下垫面子图的角二阶矩值则主要集中在 0.0365—0.2584

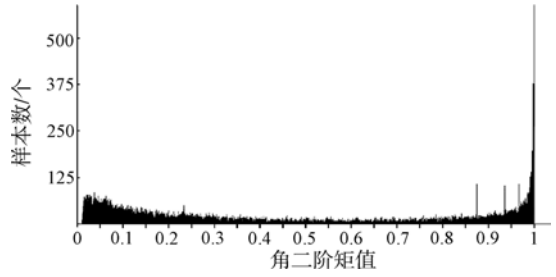

图 5　云层子图的角二阶矩值分布
(横坐标 1.0 处的角二阶矩值远超出其坐标所表示的范围)

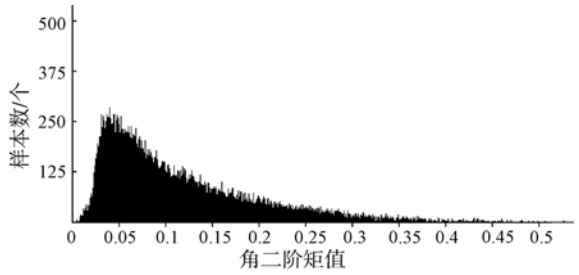

图 6　下垫面子图的角二阶矩值分布

之间。从图 5、图 6 看角二阶矩值分布对下垫面与云的区分度很高。实际算法中，云层及下垫面的角二阶矩值分布区间也会随着训练数据的增多进行调整。

3.2　基于树状判别结构的云层检测新算法

合理安排各种判别标准的次序，对分辨精确度有重要影响。灰度值是区分云区与非云区域的重要特征参数。根据物体的反射特性，通过灰度阈值即可有效的对云层和下垫面粗略划分。阈值判别会将图像中的白噪声和冰雪覆盖的地面物体误判为云，导致检测精确度的下降。这些被误判的像元点根据其上下文关系，是可以有效的排除。云与下垫面物体具有不同的纹理特征，这使得使用纹理分析的方法能够对其进行区分。在阈值判断的基础上，提取云层和下垫面的纹理特征参数，使用分形维数和角二阶矩值对图像进一步区分。分形维数和角二阶矩值从不同的方面表示了图像的纹理特征。分形模型用于描述复杂的不规则图形的自相似性，适合对不同类型物体进行分类；角二阶矩值是图像灰度分布均匀性的度量，适合于识别大面积的同类物体。利用分形维数值对云的判别的肯定性高和角二阶矩值对下垫面与云的区分性高的特点，组成树状判别，互相补充。根据上述对于各特征参数的分析以及遥感卫星图像云层特点，本文提出了一种树状判别结构，如图 7。

在云层检测树状判别结构中，首先根据光谱阈值判别法得到的阈值百分比，将待判定子图划分为极可能为云、不确定分类和非云 3 类。根据子图划分的不同类别采取不同的处理步骤。被划分到非云类别中的子图直接判定为下垫面区域。被划分到极有可能为云类别中的图像子图，需要进行分形维数的判定，进一步从纹理分析的角度对其进行确认。如果该子图的分形维数值也满足云层的特点，则判定其为云层区域；否则，进行角二阶矩值的判断以减少漏判(是云但未被判定为云)的可能性。同样的思想应用在对不确定分类子图的判定上，要注意的是不确定分类子图在光谱特征上云的特性不强，角二阶矩值用来减少误判(非云但被判定为云)的可能性。树状判别结构的优点在于对子图图像的区分可以不必计算所有的特征参数。在判别树中，叶子节点即为判别的最终结果，因此，只要沿着某一条路径走到叶子节点，即可得到判别结果。分形维数值和角二阶矩值的运算复杂度比较高，避免这两种运算将会使算法的效率明显提高。这种树状结构能够在平均意义上显著提高算法的运行效率，尤其适用于遥感图像数据量非常大的应用场景。

4　实验结果分析与应用

采用中巴地球资源卫星获得的真实遥感图像数据进行实验，从性能和判别精确度两个方面对算法进行验证。

4.1　性能

本文提出的云层检测算法由于使用了改进的分形维数计算方法和树状判别结构，其运算性能得到了显著的提高。改进的分形维数计算方法显著减少图像的遍历次数和运算操作次数。树状判别结构在平均意义上减少算法的运行时间。

4.1.1　改进的分形维数计算方法

改进的分形维数计算方法带来性能的提高主要表现在 2 个方面：第一，改进算法利用不同尺度因子划分子图的空间位置关系，通过保存中间结果，显著减少图像遍历次数，避免了大量的访存操作；第二，改进算法通过公式变换，消除了大量复杂运算。改进两种算法的比较如表 2。表中的各项数值都是以 64×64 大小子图图像为单位的统计量。

可以看到，图像由 3 次遍历完成计算优化为一次遍历操作即可完成运算，算法中运算次数尤其是复杂运算的运算次数显著减少，计算量减少了 2/3。同时，对于实现算法的具体程序也进行优化，使得

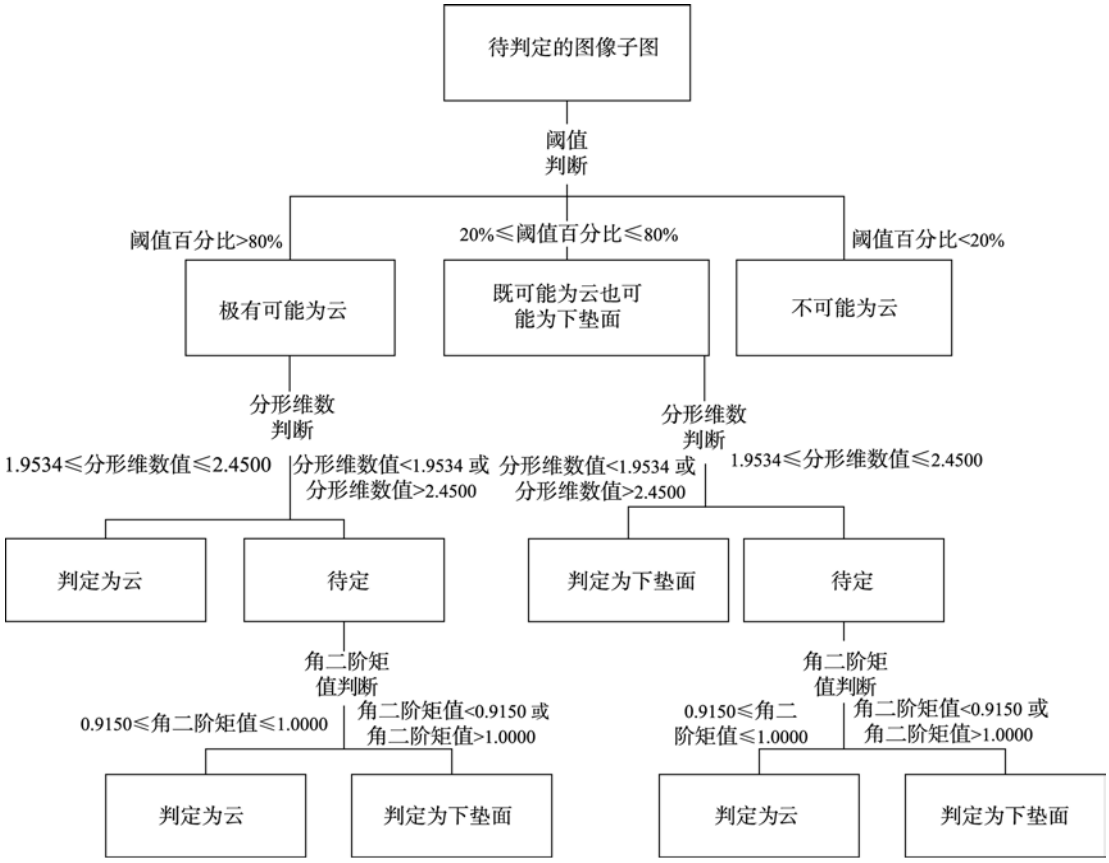

图 7　云检测算法的树状判别结构

表 2　分形维数算法改进前后的比较

	图像遍历次数	对数运算次数	乘法运算	除法运算	比较次数
原计算方法	3	18	10	1	23904
改进算法	1	2	0	0#	8160

除法操作由移位操作代替

运行效率进一步提高。选取 42120 个大小为 64×64 的遥感图像子块，总数据量为 165MB。验证环境为个人计算机，主要配置为: Pentium 4 CPU 3.06GHz; 内存 DDR2 800MHz 1.50GB。使用不同的算法进行处理所需要的时间消耗如表 3。

原始算法的误差主要来源于使用最小二乘法拟合直线斜率时产生的误差，改进算法仅仅是利用了不同尺度因子划分子图的位置关系和对原有算法的最小二乘法拟合直线斜率的计算过程进行转化和化简操作，因此，改进算法与原有算法相比结果精确度没有发生变化。

表 3　分形维数算法运行效率对比

	处理时间/s
原始算法	18.463
改进及优化后	3.313

4.1.2　树状判别结构

使用树状判别结构可以不必计算所有的特征参数就可能得到判别结果。若不使用树状判别结构，则区分每个子图要计算所有特征参量。因此，树状判别结构能够在平均意义上显著提高算法的运行效率。

由于算法的执行路径与图像中云层的覆盖密切相关，因此从 CBERS 02B 遥感卫星图像中选取 3 类典型图像: 几乎为云、几乎为下垫面和部分为云部分为下垫面的图像。每种类型选取 6 景图像，每景大小为 6132×5812。分别对使用树状判别结构和不使用树状判别结构的算法进行测试。在同样的测试环境下，每景图像经过 6 组实验，统计平均值得到的测试结果如表 4。

表 4 的结果表明在云覆盖率较低或较高的情况下，树状判别结构能够显著提高算法的运行效率，

表 4　两种判别结构的运行时间

	使用树状判别结构/s	不使用树状判别结构/s
基本无云	0.224	2.365
基本为云	0.794	2.254
部分有云	0.972	2.431

执行速度最多可以提高 10 倍以上。对于云覆盖率居中的图像，判别树也能获得较好的性能。

4.2　精确度

利用本文提出的云检测算法对遥感卫星图像进行自动检测，输出结果为遥感图像左上，右上，左下，右下 4 个子图的云覆盖率以及云区提取图。使用中巴地球资源一号 02B 真实遥感卫星图像数据，对算法的精确度进行测试。提取云检测算法判定为云层的子图，用目测的方法标定被误判的下垫面子图，统计得到算法的虚警概率；提取算法判定为下垫面的子图，用目测的方法标定被漏判的云层子图，统计得到算法的漏警概率。中巴地球资源卫星系统实际应用该算法，对遥感卫星图像进行自动云检测，结果显示虚警概率小于 5%，漏警概率小于 10%。对图 8(a)、图 9(a)中的原始图像应用算法进行云层检测，得到的实验结果如表 5。

提取并显示原始图像中的云层子图，分别如图 8(b)、图 9(b)。

为了验证该算法的通用性，选取了由另一颗工作在可见光/近红外波段的遥感卫星获取的原始图像数据，对算法进行测试。原始的遥感卫星图像如图 10(a)和图 11(a)。使用本文提出的云检测算法进行处理，得到的云覆盖百分比结果如表 6。提取并显示原始图像的云层子图，分别如图 10(b)和图 11(b)。

对比原始图像和云区提取图，可以看出云检测算法基本能够正确的分辨遥感卫星图像中的云层和下垫面物体。但图像中仍然存在一定的误判和漏判现象。误判大多出现在地面的雪区，这是因为雪区的光谱特征和纹理特征与云区极为相似。漏判主要出现在云层的边缘区域，这是因为云层的边缘处，其灰度值变化明显，纹理细节多，纹理特征与下垫面物体的纹理特征更加接近，容易误判为下垫面区域。这些问题也是将来要继续研究和改进的地方。

目前云检测的结果主要用来丢弃“无用”图像，或者产生遥感图像质量评价，其提供的丰富信息未

表 5　云覆盖率的检测结果/%

	左上子图	右上子图	左下子图	右下子图
图 8(a)	37.15	99.58	55.26	84.69
图 9(a)	83.26	88.39	14.35	3.84

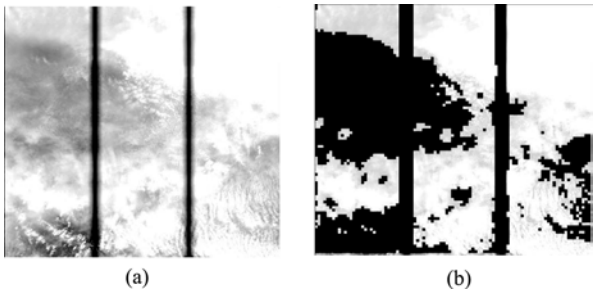

图 8　CBERS 02B 获取的平原地区遥感图像
(a)原始图像; (b)云区提取图

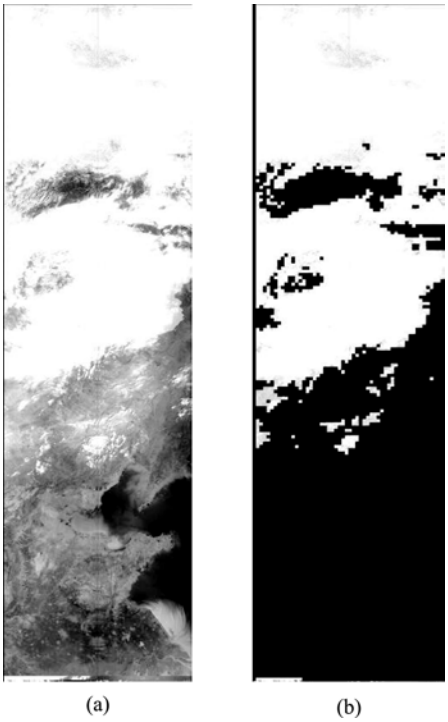

图 9　CBERS 02B 获取的山区遥感图像
(a)原始图像; (b)云区提取图

表 6　云覆盖率的检测结果/%

	左上子图	右上子图	左下子图	右下子图
图 10(a)	31.50	90.29	66.17	85.13
图 11(a)	13.11	77.46	95.91	97.57

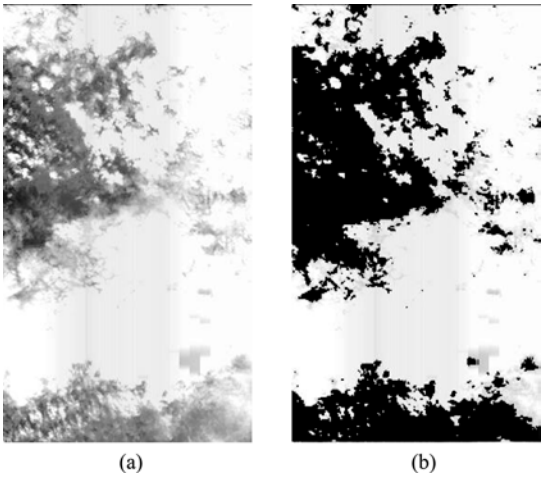

图 10　光学遥感卫星获取的高原地区遥感图像
(a)原始图像; (b)云区提取图

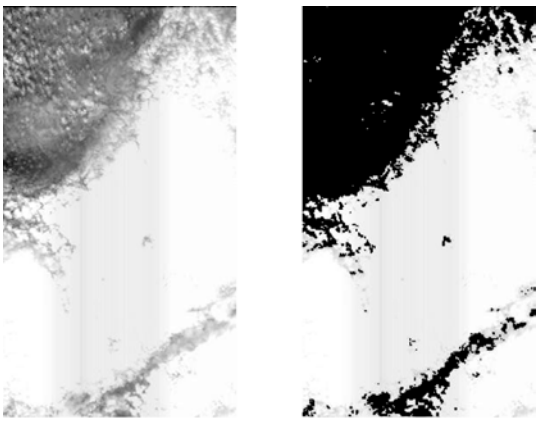

(a) (b)

图 11 光学遥感卫星获取的平原遥感图像
(a)原始图像; (b)云区提取图

得到有效的利用。针对遥感卫星系统资源有限，处理数据量大的特点，如何利用云检测算法提供的信息，进一步提高系统资源的利用率和系统性能，成为一个重要的课题。

利用云检测结果产生的图像质量评价，选择性的压缩或丢弃数据，可以节省存储资源，节约下传带宽，降低对卫星图像处理系统的压力，是提高系统资源利用率和系统性能的一种有效策略。除了从系统资源和性能的角度考虑，还可以利用云检测结果提高图像的有用率(Algra, 2002)。云检测的结果信息结合数字天气模型或者气象卫星获得的历史数据，能够有效的预测云层的覆盖情况，从而制定一种云避免机制，提高图像本身的有用率。两种实现云避免机制的方法是选择成像和云编辑。选择成像方法是传感器根据云层预测情况有选择的在那些没有云的区域获取遥感图像；云编辑方法是将遥感图像中被云覆盖的部分丢弃，或者使用一个无云波段的图像数据代替，或者用低分辨率表示。另外云检测结果还可以用于增加光学设备的成像效率。如果根据云层检测结果，主动调整遥感平台成像设备的光轴指向，使传感器能够动态选择无云的区域获取遥感图像，则可以获得潜在的更高的系统效率(Algra, 2003)。

5 结 论

本文详细介绍了图像云层检测算法中光谱阈值判别法和纹理分析法的基本原理，研究了各个判别标准对分辨精确度的影响。提出了一种改进的分形维数计算方法，能在不影响精确度的前提下使算法性能提高 5 倍左右。在综合分析各个判别标准对精确度影响的基础上，提出了树状判别结构，合理安排各个判别标准的优先级，形成一个准确高效的云层判别算法。通过编程实现算法，选取真实的卫星遥感图像对算法进行验证，得到了较好的分辨精确度。算法实现简单，运算速度快，基本能够满足遥感平台对于实时性的要求。最后，描述了如何应用云检测算法的结果，挖掘潜在的利用价值，充分利用系统各种资源，使遥感平台系统能够在现有的资源条件下提供更高的性能。

REFERENCES

Ding B H, Li W C and Wang F M. 1999. Analysis of fractal image and design of fractal dimension calculation program. *Journal of University of Science Technology Beijing*, **21** (3): 304—307

Gonzalez R C and Woods R E. 2006. Digital Image Processing. Beijing: Publishing House of Electronic Industry

Li B C. 2006. Texture feature retrieval and applications using gray co-occurrence matrices. *Journal of Kashgar Teachers College*, **27** (6): 35—37

Li M, Liew S C and Kwoh L K.2003. Producing cloud free and cloud-shadow free mosaic from cloudy IKONOS images. Geoscience and Remote Sensing Symposium Proceedings

Li Y C, Sun H, Xu M and Zhang X H. 2003. Box-counting method and its application to the detection of fog using GMS-5 weather satellite data. *Bulletin of Sciences and Technology*, **19** (1): 29—31

Liu Z G, Li Y X and Huang F. 2007. Cloud detection of MODIS satellite images based on dynamical cluster. *Remote Sending Information*, **4**: 33—35

Loyola D. 1998. A new cloud recognition algorithm for optical sensors. Geoscience and Remote Sensing Symposium Proceedings

Luis G C, Gustavo C V, Julia A, Jose D M, Javier C, Luis A, Luis G, Juan C F and Jose M. 2006. Cloud detection for MERIS multispectral images. Geoscience and Remote Sensing Symposium Proceedings

Song X N and Zhao Y S. 2003. Cloud detection and analysis of MODIS image. *Journal of Image and Graphics*, **8** (9): 1079—1083

Takayasu H. 1990. Fractals in The Physical Sciences. Manchester: Manchester University Press

Theo Algra. 2002. On the effectiveness of cloud cover avoidance methods in support of the supper-spectral mission for land applications. Geoscience and Remote Sensing Symposium Proceedings

Theo Algra. 2003. Real-time cloud sensing for efficiency improvement of optical high-resolution satellite remote sensing.

Geoscience and Remote Sensing Symposium Proceedings.

Wang R F, Sun L, Zhang J and Song P J. 2006. The application analysis of spectrum threshold and MSC cloud detection algorithms based on “HY-1A” CCD data. *Acta Oceanologica Sinica*, **28** (6): 158—163

Yu W X, Cao X G, Xu L and Mohamed B. 2006. Automatic cloud detection for remote sensing image. *Chinese Journal of Scientific Instrument*, **27** (6): 2184—2186

Zhang Z, Dong F Aand Wu Y L. 2005. Estimation of fractal dimension for 2-D gray image. *Computer Applications*, **25** (12): 2853—2854

附中文参考文献

丁保华，李文超，王福明. 1999. 分形图像分析与分形维数计算程序的设计. 北京科技大学学报, **21**(3): 304—307

李丙春. 2006. 基于共生矩阵的图像纹理特征提取及应用. 喀什师范学院学报, **27**(6): 35—37

李亚春，孙涵，徐萌，张旭辉. 2003. 计盒维数法在云雾遥感检测中的应用研究. 科技通报, **19**(1): 29—31

刘志刚，李元祥，黄峰. 2007. 基于动态聚类的 MODIS 云检测算法. 遥感信息, **4**: 33—35

宋小宁，赵英时. 2003. MODIS 图像的云检测及分析. 中国图像图形学报, **8**(9): 1079—1083

王瑞富，孙凌，张杰，宋平舰. 2006. 基于光谱阈值法和分裂合并聚类算法的“ HY-1A ”CCD 云检测算法和应用. 海洋学报, **28**(6): 158—163

郁文霞，曹晓光，徐琳, Mohamed Bencherkei. 2006. 遥感图像云自动检测. 仪器仪表学报, **27**(6): 2184—2186

张志，董福安，伍友利. 2005. 二维灰度图像的分形维数计算. 计算机应用, **25**(12): 2853—2854